Heliospheric evolution of solar wind small-scale magnetic flux ropes

M. L. Cartwright[1] and M. B. Moldwin[2]

Received 18 March 2009; revised 26 March 2010; accepted 6 April 2010; published 10 August 2010.

[1] We present results from the first comprehensive small-scale flux rope survey between 0.3 and 5.5 AU using the Helios 1, Helios 2, IMP 8, Wind, ACE, and Ulysses spacecrafts to examine their occurrence rate, properties, and evolution. Small-scale flux ropes are similar to magnetic clouds and can be modeled as a constant-alpha, force-free, cylindrically symmetric flux rope. They differ from magnetic clouds in that they have durations on the order of tens of minutes up to a few hours, they lack an expansion signature at 1 AU, and they do not have a depressed proton temperature compared to the surrounding solar wind plasma. The occurrence rate of small-scale flux ropes is slightly higher in the inner heliosphere than the outer heliosphere and has a weak dependence on the phase of the solar cycle. The duration of the events as a function of radial distance indicates there is a large, rapid expansion within 1 AU and it becomes constant in the outer heliosphere. This behavior implies small-scale flux ropes are created and nearly complete their evolution within 1 AU.

Citation: Cartwright, M. L., and M. B. Moldwin (2010), Heliospheric evolution of solar wind small-scale magnetic flux ropes, *J. Geophys. Res.*, *115*, A08102, doi:10.1029/2009JA014271.

1. Introduction

[2] Magnetic flux ropes are a common phenomenon in the heliosphere. They are created on the Sun, in the Earth's magnetotail, and at other planets. They can be described as a bundle of magnetic field lines twisted into a tube-like shape with a strong axial field. In the outer section of the rope, the twisted field is strongest while the axial field lines become dominant in the inner section. In cylindrical coordinates, the axial field is called the core field of the flux rope and the azimuthal field is called the twist or bipolar field of the flux rope.

[3] Magnetic flux ropes are important because they transport field and plasma from one location to another. The scale size of a flux rope is dependent on the environment in which it was created and its subsequent expansion. For example, in the Earth's magnetotail, flux ropes have scale sizes on the order of 17 R_E. They are commonly believed to be created by magnetic reconnection across the magnetotail plasma sheet [*Moldwin and Hughes*, 1992].

[4] A large-scale flux rope originating at the Sun is called a magnetic cloud (MC) and has been defined as: (1) a smooth magnetic field rotation parallel to a plane, (2) enhanced magnetic field strength compared to the surrounding solar wind, and (3) a depressed proton temperature [*Burlaga et al.*, 1981]. These events have been well-studied from 0.3 to 5.5 AU [e.g., *Klein and Burlaga*, 1982; *Bothmer and Rust*, 1997; *Bothmer and Schwenn*, 1998; *Mulligan et al.*, 1998; *Lepping et al.*, 1990, 2006; *Lynch et al.*, 2005; *Lepping and Wu*, 2007]. They are on average 21 h in duration, varying between 8 and 48 h at 1 AU. The axial field strength is typically greater or equal to twice the background field. The occurrence frequency per year has a low correlation with the monthly sunspot number, based on observations from 1995 to 2003. At 1 AU, MCs usually have a decreasing velocity profile across the duration of the event. This implies that they are still expanding into the solar wind and are not in pressure balance [e.g., *Lepping et al.*, 2006].

[5] The most utilized flux rope model is called the static constant-alpha, force-free, cylindrically symmetric field geometry [i.e., *Goldstein*, 1983; *Burlaga*, 1988]. The force-free condition implies there are no gravitational or thermal pressure gradient forces and the structure is in steady state allowing $\nabla \times \vec{B} = \mu_0 \vec{J} = \alpha \vec{B}$. Assuming alpha is constant, *Lundquist* [1950] showed this equation has solutions of Bessel functions as seen in equation 1.

$$B_R = 0 \qquad \text{Radial component} \tag{1a}$$

$$B_T = B_0 H J_1(\alpha R) \qquad \text{Tangential component} \tag{1b}$$

$$B_A = B_0 J_0(\alpha R) \qquad \text{Axial component} \tag{1c}$$

where B_0 is the field magnitude on the axis, $R = r/R_0$ where R_0 is the radius of the cloud, and r is the radial distance from the cloud axis. J_0 and J_1 are the zeroth- and first-order Bessel functions. $H = \pm 1$ and defines the sign of magnetic

[1]Space Sciences Laboratory, University of California, Berkeley, California, USA.
[2]Department of Atmospheric, Oceanic, and Space Sciences, University of Michigan, Ann Arbor, Michigan, USA.

0148-0227/10/2009JA014271

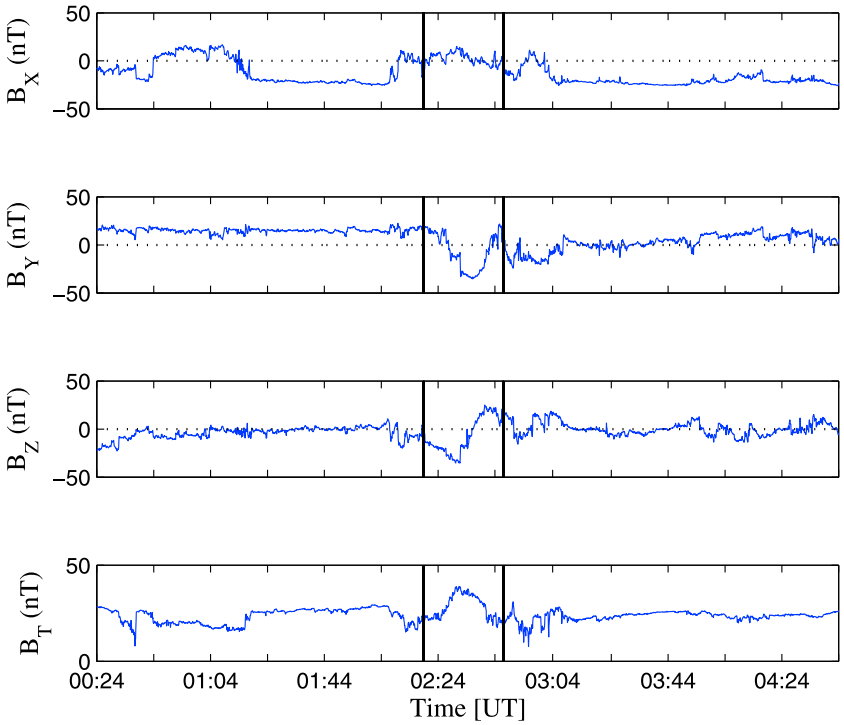

Figure 1. An example of a small-scale flux rope found at 0.39 AU. It was identified from the Helios 1 data set on 4 March 1975 from 0219 to 0247 UT. The black vertical bars indicate the boundaries of the event.

helicity of the flux rope. The flux rope boundaries are defined to be the first zero of the zeroth Bessel function, where $r = R_0$ and the value of α is 2.40. The magnetic helicity is a measure of how twisted the field has become and the handedness. Many interplanetary coronal mass ejections (ICMEs) will not fit the classic MC criteria and require more advanced models. If the structure is not force-free or cylindrically symmetric, then the use of a symmetric, static model will give large errors and many interesting events will be excluded from the data set, e.g., the MC-like events from the work of *Lepping et al.* [2006]. There have been models focused on cases where alpha is not constant [e.g., *Farrugia et al.*, 1995; *Osherovich et al.*, 1999; *Vandas et al.*, 1993; *Mulligan*, 2002] but such models are often designed to model the magnetic cloud evolution. They are not valid at particular stages of evolution.

[6] MCs are large structures and it is common to study them using hourly data sets. However, hourly averages cannot be used to study phenomena with timescales of the order of tens of minutes to hours. The solar wind small-scale flux ropes identified by *Moldwin et al.* [1995, 2000] are such a phenomenon. These structures were first discovered by *Moldwin et al.* [1995] with the Ulysses spacecraft near 5 AU. The one event identified was characterized by a bipolar field rotation coincident with a strong axial core field with duration of 4 h. This event motivated a small survey at 1 AU for small-scale flux ropes, where *Moldwin et al.* [2000] identified six events with the Wind and IMP 8 magnetic field data sets. These events all have bipolar field rotations coincident with a core field enhancement and were on the order of tens of minutes duration and displayed the signature of a force-free, symmetric magnetic flux rope.

[7] Small-scale solar wind flux ropes have recently been extensively studied at 1 AU [*Cartwright and Moldwin*, 2008; *Feng et al.*, 2007, 2008]. A classic example of a small-scale flux rope (as shown in Figure 1) was observed by Helios 1 at 0.39 AU. The magnetic field vectors are shown in solar ecliptic (SE) coordinates. This is a heliocentric coordinate system where B_x points from the spacecraft to the Sun, B_z is normal to and northward from the ecliptic plane, and B_y completes the right-handed set. The magnetic field topology is similar to a magnetic cloud, where in Figure 1 the core field is in B_Y SE coincident with a bipolar field observed in B_z SE component. The B_x SE component is flat consistent with the Lundquist solution shown in equation (1).

[8] Given that the magnetic field topology is similar to magnetic clouds, the search parameters used to identify small-scale flux ropes involved strong core fields associated with a bipolar field in one of the components. The studies by *Feng et al.* [2007, 2008] visually identified events from the years 1995 to 2005 and the study by *Cartwright and Moldwin* [2008] used an automated technique to identify events from 1995 to 2005. There was little overlap between the lists because the automated technique [*Cartwright and Moldwin*, 2008] quantitatively searched for strong core fields. The majority of the events identified by the visual survey by *Feng et al.* [2007] had weaker core field peaks than the automated survey identified. Upon further examination by *Cartwright and Moldwin* [2008], these weaker core field flux ropes found by *Feng et al.* [2007] were often consistent with compressive Alfvén waves. At these small-scale sizes, there are solar wind disturbances called com-

pressive Alfvén waves (or fast mode waves) that can have enhanced total field intensity and a similar magnetic field signature [*Burlaga and Turner*, 1976]. These events are identified by a cross correlation of the magnetic field and velocity field vectors due to the Alfvén wave property that for an isotropic plasma, $\mathbf{v} = \pm (V_A/B_0)\mathbf{b}$. The vectors **v** and **b** are the perturbations of velocity and magnetic field, B_0 is the average field strength, and V_A is the Alfvén speed defined to be: $V_A = B/(\mu_0\rho)^{1/2}$. Studies investigating small-scale flux ropes should exclude these events because the magnetic signatures are identical.

[9] The comprehensive surveys at 1 AU [*Cartwright and Moldwin*, 2008; *Feng et al.*, 2007; 2008] indicated a population of small-scale flux ropes that dominates in occurrence frequency over large-scale flux ropes (or MCs) identified from the *Lepping et al.* [2006] database and maintained online at http://lepmfi.gsfc.nasa.gov/mfi/mag_cloud_pub1.html. These three databases [*Cartwright and Moldwin*, 2008; *Feng et al.*, 2007, 2008; *Lepping et al.*, 2006] all used Wind data that included some data gaps. Although the magnetic topology of small-scale flux ropes is similar to MCs, these structures differ from MCs in several key ways. Small-scale flux ropes have durations on the order of tens of minutes to several hours and scale sizes on the order of a few hundred Earth radii (0.001–0.003 AU), where MCs are on the order of 20 h and a quarter of an AU in size. Small-scale flux ropes have constant temperature profiles similar to the surrounding solar wind, unlike MCs that have depressed proton temperatures. At 1 AU, they show little expansion unlike MCs, indicating they are at their evolutionary endpoint [*Cartwright and Moldwin*, 2008]. These differences suggest that they may have different origins, with MCs formed in the lower corona and small-scale magnetic flux ropes forming in the solar wind.

[10] These past surveys at 1 AU and the differences from MCs motivate the current study of the radial evolution of small-scale magnetic flux ropes in the solar wind from 0.3 to 5.5 AU. Ideally, to study the evolution of a small-scale flux rope, the same event should be examined with a spacecraft at various heliospheric distances. We searched the various data sets for such an event but found no event observed by widely separated spacecrafts between 0.3 and 1 AU or 1 and 5.5 AU. This survey presents the results of small-scale flux ropes identified at various heliospheric distances to understand the collective behavior of these objects from the inner to middle heliosphere. This study answers the questions: Are these small-scale flux ropes observed at all radial distances from the Sun? Do they have the same properties at all distances? Do the answers to the questions provide clues to their origins and formation mechanism?

2. Methodology

2.1. Spacecraft Used in This Survey

[11] We examined Helios 1, Helios 2, IMP 8, Wind, ACE, and Ulysses magnetic field and plasma data sets available from the National Space Science Data Center, the Space Physics Data Facility, and the solar wind data set compiled to develop a solar wind data set (propagated to the bow shock or not propagated) by J. Weygand at UCLA (http://www.igpp.ucla.edu/jweygand/htmls/Propagated_SW.html).

[12] Helios 1 and Helios 2 were launched in December 1974 and January 1976, respectively, into a heliocentric orbit that ranged from 0.3 to 1 AU. For more information on the instrumentation and data analysis of the magnetometer experiment, see the work of *Scearce et al.* [1975], and for the plasma experiment, see the work of *Rosenbauer et al.* [1977]. The magnetic field data are available from 15 December 1974 to 16 June 1981 in SE spacecraft-centered coordinates and contain many data gaps.

[13] IMP 8 was one of a series of probes used to investigate Earth's magnetosphere and the solar wind. The IMP 8 data used in this study were from 1975 to 1994, where the spacecraft was in an approximate 12.5 day geocentric orbit. This time period was used to extend the data set between Helios and the start of the Wind mission and provide a 1 AU set of observations that overlap with the Helios data over a solar cycle. IMP 8 was in the solar wind from 7 to 9 days out of the 12.5 orbit. The data coverage in the solar wind was around 60% but contained many small (approximately tens of minutes) data gaps, which decreased the usable coverage for locating small flux ropes to around 45%, depending on the year. The Goddard Space Flight Center magnetometer and the Massachusetts Institute of Technology and Los Alamos National Laboratory plasma data sets used in this study were in geocentric SE (GSE) coordinates at a time resolution of 1 min.

[14] The Wind spacecraft was launched in November 1994 to measure the solar wind and Earth's foreshock. Following a double lunar swingby, Wind was placed in a halo orbit around the first Lagrangian (L1) point allowing for sampling of the incoming solar wind at Earth and spent time in petal orbits near the Earth and the Moon. The magnetic field and plasma data sets used were when Wind was in the solar wind and are described by *Lepping et al.* [1995] and *Ogilvie et al.* [1995], respectively. We used data in GSE coordinates at a 1 min resolution for years 1995 to 2007.

[15] ACE was launched in August 1997 as a solar wind monitor at L1. We used data from 1997 to 2007 in GSE coordinates at 1 min time resolution. For more information on the magnetic and plasma experiments, see the work of *Smith et al.* [1998] and *McComas et al.* [1998].

[16] Ulysses was launched in October 1990 with the primary purpose to investigate the solar wind, neutral gases, and energetic particles as a function of solar latitude. After launch, Ulysses cruised to Jupiter in the ecliptic plane and used the Jupiter flyby to achieve a heliospheric orbit over the solar poles. We will only present results of small-scale flux ropes found in the ecliptic plane. At higher latitudes, out of the ecliptic plane, the solar wind is composed almost entirely of the fast solar wind (>600 km s^{-1}). Within the fast solar wind shear, Alfvén waves are found to be almost continuous [*Smith et al.*, 1995] from less than 1 h up to 10 h in scale size [*Bruno et al.*, 1985]. These waves are at the same time and length scales as small-scale flux ropes and share the same magnetic field signature of a bipolar field. This problem will limit the number of small-scale flux ropes found in the fast wind. Because of the Alfvénic nature of the fast wind, there will be a bias in the selection of small-scale flux ropes toward being in the slow wind. Because of the similarities in the magnetic signature and the near-continuous spectrum of these Alfvén waves, identifying small-scale

flux ropes is extremely difficult out of the ecliptic plane. We used data from when Ulysses was in cruise to Jupiter and the three subsequent aphelion passes at 5.4 AU (within ± 10° of the solar ecliptic plane, which is 2.9° and −17.2° in heliographic latitude). These passes were during the time periods 5 March 1992 to 17 September 1992, 18 October 1997 to 27 November 1998, and 26 December 2003 to 30 January 2005. Information on the magnetic and plasma data experiments can be found in the work of *Balogh et al.* [1992] and *Bame et al.* [1992]. In this study, the data were in radial-tangential-normal (RTN) coordinates at 1 (4) min time resolution for the magnetic (plasma) data, respectively.

2.2. Selection Criteria

[17] The small-scale flux rope selection was done in three parts: (1) a visual survey of the solar wind magnetic field data sets, (2) a removal of compressive Alfvén waves, and (3) a model validation of the events.

[18] We visually examined the magnetic field data sets using an approximate 10 h window. We decided to proceed with a visual survey over an automated identification method [*Cartwright and Moldwin*, 2008] primarily because it was difficult to adapt the program to manage the data gaps from the Helios and IMP 8 data sets. We wanted to survey all the data sets in the same manner, so we used a visual survey with a wave removal method for this study. We used the force-free cylindrically symmetric flux rope property of an inflection point located at or near the peak of the axial core field in the small-scale flux rope [*Moldwin et al.*, 2000]. We first identified an inflection point in the B_Y or B_Z coordinate coincident with a core field peak in the remaining component (B_Y or B_Z). The boundaries of an ideal magnetic flux rope are current sheets that often can be observed as minima in the total field component and/or a directional discontinuity separating the flux rope structure from the surrounding solar wind plasma. We identified boundaries by either (1) locating the start and end of the total magnetic field enhancement relative to the background field strength as the beginning and end of the flux rope, (2) using the minima associated with the core field component enhancement, or (3) using the maxima of the bipolar field. After boundary identification, we applied minimum variance analysis (MVA) to the SE, GSE, or RTN coordinates in which the maximum coordinate was the field rotation and the intermediate coordinate was the axial core field [*Lepping et al.*, 1990]. Our standards were such that the maximum eigenvector (λ_1) divided by the minimum eigenvector (λ_3) must be equal to or greater than six and the intermediate eigenvector (λ_2) divided by the minimum eigenvector (λ_3) must be equal to or greater than two, which will guarantee well determined MVA directions [*Sonnerup and Cahill*, 1967; *Burlaga and Behannon*, 1982]. We excluded events if the bipolar field was primarily in the B_X GSE; B_R RTN; B_X SE coordinate as to remove any potential heliospheric current sheet crossings. However, we include events that had B_X crossings if the bipolar field was primarily in one of the other two coordinates (as indicated by the maximum eigenvector).

[19] The second step in our selection process was the removal of compressive Alfvén wave-like events; at these small scales, there are several disturbances that can bias surveys unless taken into account. As described in section 1., the magnetic field and velocity components were examined to see if they were correlated. If the correlation coefficient was ≥0.7, suggestive of Alfvénic waves, we excluded the event from the flux rope database. From the initial database of the combined ACE, Wind, IMP 8, and Ulysses events, one third of candidate small-scale flux ropes had Alfvénic properties and were removed from the final database. Those events will be the subject of a future study, but their relative high occurrence indicates that they should be carefully excluded in studies of flux ropes. The inclusion of these events has led to differences between data sets of solar wind flux ropes.

[20] The events were then validated using the nonlinear least squares method. The data were fitted to the force-free, cylindrically symmetric flux rope model discussed in the introduction. We used the same method as described in *Lepping et al.* [1990]. In this study, we did not use the assumption that the spacecraft passes through the center of the flux rope but used the nonlinear, least-squares minimization of the data to the force-free, cylindrically symmetric flux rope model using five free parameters: the flux rope longitude (φ) and latitude (θ), the impact parameter (p), axial field strength (B_o), and the sign of the helicity (H). The χ^2_{DIR} error from the model fit of the flux rope axis is used to evaluate the goodness of fit, where an error >0.3 is typically a poor fit [*Lepping et al.*, 1990]. We labeled events as flux ropes if the error was up to 0.5. The flux rope axis can have any orientation (ϕ_{Rope}, θ_{Rope}) relative to the ecliptic plane. The observed directions of the magnetic field at the leading edge, center, and trailing edge of the flux rope are commonly used to classify magnetic clouds [*Bothmer and Rust*, 1997; *Bothmer and Schwenn*, 1998; *Mulligan et al.*, 1998]. There are two broad classifications, the first is where the flux rope axis lies in the ecliptic plane (e.g., in the B_Y GSE component) and the second where the axis lies out of the ecliptic plane (e.g., in the B_Z GSE component). We have classified our events in the same manner. In this study, we are interested in the basic properties of the flux ropes; their orientation; duration of the event, which is slightly modified from the original visual boundaries because of the least-squares minimization technique; and the strength of the axial field extracted from the model.

3. Results

3.1. Examples of Small-Scale Flux Ropes at Various Radial Heliospheric Distances

[21] We identified 23 small-scale flux ropes from the Helios 1 and Helios 2 data sets, 66 flux ropes from the IMP 8 data set, 91 flux ropes from the Wind data set, 70 flux ropes from the ACE data set, and 20 flux ropes from the Ulysses data set. There were 51 events identified in both the Wind and ACE databases and 12 events found in the ACE data set but not in the Wind data set. We excluded the unique ACE events and created a combined 1 AU database using the Wind and ACE events that contains a total of 98 unique flux ropes. There are a total of 219 unique small-scale flux ropes at radial distances from 0.3 to 5.5 AU. The flux ropes range in duration from 0.22 to 10.35 h. There are several flux ropes in our database that have been previously identified [*Feng et al.*, 2007, 2008; *Cartwright and Moldwin*, 2008; *Jian et al.*, 2008]. The Helios 1 and Helios 2, IMP 8,

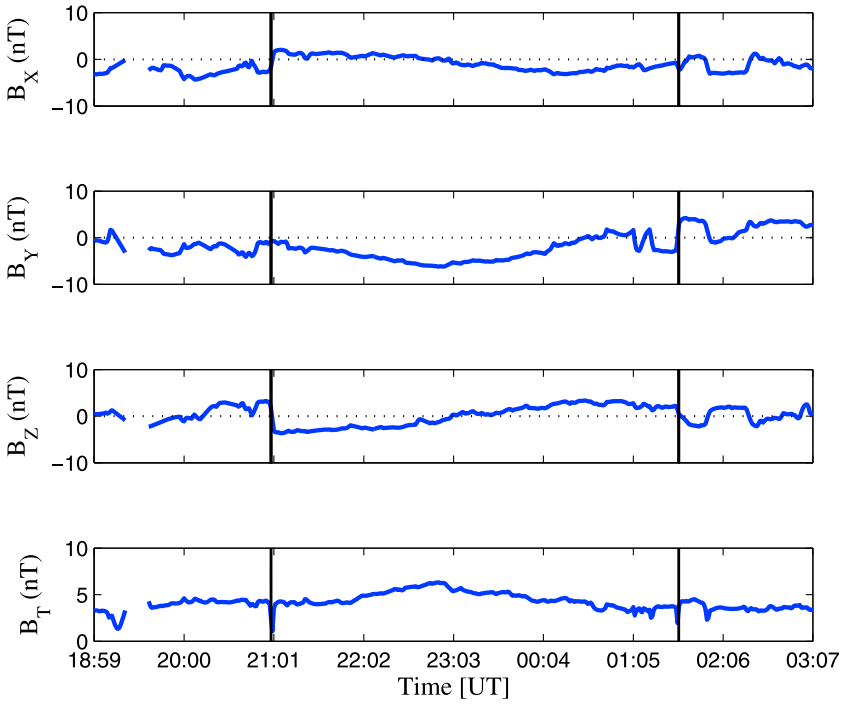

Figure 2. A classic example of a small-scale flux rope located at 1 AU. It was identified from the Wind data set from 11 August 1996 at 2059 to 12 August 1996 0136 UT. The boundaries are represented by the solid vertical lines.

and ACE/Wind combined database and Ulysses small-scale flux rope database can be found in Appendix A, Table A1.

[22] We present three examples at 0.3, 1, and 5 AU radial distances. The first flux rope presented in Figure 1 was observed by the Helios 1 spacecraft on 4 March 1975 from 02:19 to 02:47 UT. The axial core field strength was 35 nT. The duration of the event was 0.47 h. It was observed at a heliospheric distance of 0.39 AU. The hourly plasma data indicate it was located in the fast solar wind with a speed of 630 km s^{-1}. The λ_1/λ_3 ratio was 21 and the λ_2/λ_3 ratio was 16. The ratio of the axial field strength to the average 6 h surrounding the flux rope was 1.8. The orientation of the flux rope was such that the leading field from the bipolar signature is in the south direction and the trailing field is in the north direction. The axial field is in the west direction, so the event is an SWN event. The flux rope is a right-handed event and is embedded in the away interplanetary magnetic field (IMF) polarity sector. The longitude of the axis is 280° and the latitude is −25°, with respect to the ecliptic plane.

[23] The second example presented in Figure 2 was identified with the Wind spacecraft starting on 11 August 1996 at 20:59 UT to 12 August 1996 at 01:36 UT. The duration of the event was 4.62 h. The axial field strength was 5.34 nT. The λ_1/λ_3 ratio was 50.7 and the λ_2/λ_3 ratio was 12.3. The average solar wind speed over the duration of the event was 350 km s^{-1}. The latitude and longitude of the axis is 76° and −17°. The flux rope is again classified as an SWN event with a right handedness.

[24] The third example was found by the *Ulysses* spacecraft at 5.3 AU from 28 November 2004 at 06:05–07:55 UT and is presented in Figure 3. The axial field strength is 0.74 nT and the axial field strength divided by the surrounding 6 h field strength is 1.07. The duration is 1.83 h. The average solar wind speed over the duration of the event was 427 km s^{-1}. The λ_1/λ_3 ratio was 156 and the λ_2/λ_3 ratio was 7. The flux rope longitude and latitude are 77° and −3°. The flux rope is orientated such that it is SEN event with a left handedness.

3.2. Basic Properties at 1 AU and Heliospheric Evolution Statistics of Small-Scale Flux Ropes

[25] We used the Helios 1, Helios 2, IMP 8, Wind/ACE, and Ulysses small-scale flux rope database to study the number of events observed per year and how their properties depend on heliospheric distance. How frequently small-scale flux ropes are observed is a fundamental property that gives clues to their possible origin. The occurrence of small-scale flux ropes over solar cycles 21, 22, and 23 is presented in the upper plot of Figure 4. We plotted the number of events normalized by number of spacecraft months of observation per year represented as black diamonds. We used this normalization because of the deviations in spacecraft coverage from the various data sets used. The error bars are the plus and minus square root of (the number of events) divided by the months of observations per year. The solid gray line connecting the solid circles is the mean annual sunspot number per year. This plot shows a trend of small-scale flux rope occurrence, with the events most likely observed during solar minimum than solar maximum. We used these observations to create the average number of flux ropes per month of observation for cycles 21 to 23 as a function of solar cycle, shown in the lower plot of Figure 4. This analysis summed over observations at the same phase of the solar cycle in each cycle (e.g., t, $t + 11$, and $t + 22$), and then we plotted the average rate (black diamonds). For example, the first bin is the average number of flux ropes for

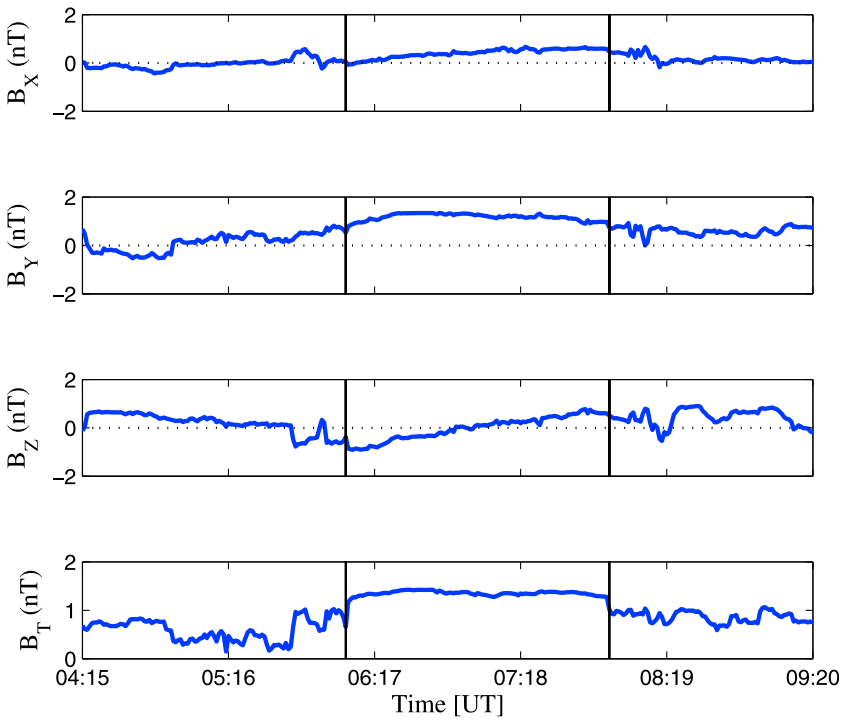

Figure 3. An example of a small-scale flux rope located at 5.3 AU. This event was identified from the Ulysses data set starting on 28 November 2004 at 0605 to 0755 UT. The boundaries are represented by the solid vertical lines.

years 1974, 1974 + 11, and 1974 + 22 divided by the average number of months of observation for those years. The error bars are the (average number of flux ropes) divided the average months of observation. The sunspot number (solid gray line) is the average number of sunspots for that year from the cycles 21 to 23. This plot does not include the year 2007 because the Sun started going into an extended minimum and it does not fit with the previous two cycles. This plot shows the same trend as the upper plot, where there are more small-scale flux ropes observed during solar minimum than maximum. The average number of events around solar minimum (taken as years 1, 2, 10, and 11 in the cycle) is one flux rope per month. The average number of events around solar maximum (here taken as years 5 through 7) is 0.4 flux ropes per month. This average trend shows that there is a tendency to observe more small-scale flux ropes during solar minimum than maximum.

[26] The number of small-scale flux ropes normalized by months of observation as a function of radial heliospheric distance is presented in Figure 5. The error bars are the square root of the (number of events) divided by the months of observation. The first column in Table 1 specifies the four regions examined: the inner heliosphere (0.3–0.75 AU), near 1 AU (0.75–1.5 AU) where we have the most months of observations, and then the outer heliosphere, which we have separated into 1.5–4.5 and 4.5–5.5 AU. There are not many events in the 1.5–4.5 AU bin because of lack of spacecraft observing hours, but the events follow the same trend as the 4.5–5.5 AU bin. In the inner heliosphere, the number of events per month is 0.8, which declines to 0.6 at 1 AU and further declines to 0.4 in the outer heliosphere (5 AU). The dashed black line is the least squares fit of the function (R^{-x}) to the data, where x indicates how fast the distribution falls off with heliospheric distance. In this case, the distribution falls as $R^{-0.24}$, indicating the number of flux ropes as a function of heliospheric distance is not flat. There is a small decrease in the occurrence frequency as a function of radial distance with more events in the inner heliosphere (0.3–1 AU) compared to the outer heliosphere (5 AU).

[27] The duration and scale size of small-scale events as a function of heliospheric distance are presented in Figure 6. The upper plot shows the average flux rope duration per heliospheric bin indicated by the black diamonds and the individual flux rope durations that created the average are plotted in gray. In the inner heliosphere, the average duration is 1.5 h. The average duration is 2.5 h at 1 AU and flattens to 4 to 4.3 h in the outer heliosphere. The dashed black line is the least squares fit of the function (R^x) to the average duration data; this indicates how the rate at which the duration increases as a function of heliospheric distance. The fit to the data is $R^{0.37}$, indicating the duration in the inner heliosphere has a large increase and then increases more slowly with increasing heliocentric distance. The lower plot shows the average scale size (in units in AU) as a function of heliospheric bin, plotted as the black diamonds. The average flux rope scale size in the inner heliosphere (<0.75 AU) is 0.0132 AU (311 R_E), at 1 AU it is 0.0247 AU (582 R_E), and in the outer heliosphere (5 AU) it is 0.0383 AU (900 R_E). The dashed black line is the least squares fit of the average data to the function R^x. The fit is found to be $R^{0.43}$. These plots show a trend where an average event in the inner heliosphere is smaller in duration and scale size than an average event at 1 AU and beyond.

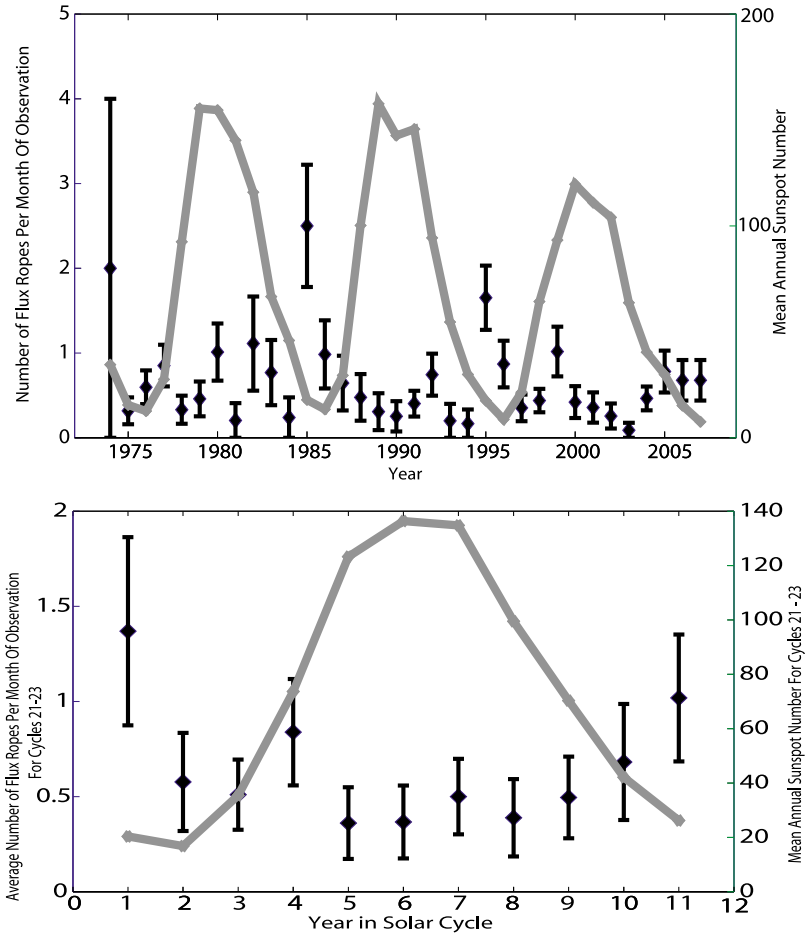

Figure 4. The upper plot is the number of small-scale flux ropes normalized by the months of observations per year from 1974 to 2007, covering solar cycles 21 to 23. The diamonds are representative of the number of events per month of observation per year. The error bars are the square root of the (number of events) divided by the number of months of observation per bin. The solid gray line represents the mean annual sunspot number. The bottom plot is the average number of small-scale flux ropes per months of observation over solar cycles 21 to 23.

[28] One of the parameters of the cylindrically symmetric model fit was the axial core field strength. This parameter was extracted and binned as described in Table 1. The average axial core field strength of the small-scale flux ropes as a function of heliospheric distance is presented in the upper plot of Figure 7. The error bars are plus and minus the standard deviation of the average axial core flux rope field strength divided by the square root of the number of events. In the inner heliosphere, the first bin, the average axial core field was 17 nT, rapidly decreased to 7 nT at 1 AU, and then flattened to approximately 2 nT in the outer heliosphere. The black dashed line is the least squares fit of the data to the function (R^{-x}), where the result found is $R^{-0.94}$. The ratio of the axial core field strength to the surrounding background interplanetary field strength determines how strong the small-scale flux rope is compared to the IMF it resides in. The average ratio of axial core field strength to background solar wind IMF as a function of heliospheric distance is present in the lower panel of Figure 7. The ratio is slightly larger in the inner heliosphere at 1.3 and is flat from 1 to 5 AU at around 1.1. The least squares fit of the data to the function (R^{-x}) is found to be $R^{-0.07}$. This distribution and the error bar size between the data points indicate the strength of small-scale flux ropes relative to the background solar wind is roughly constant from the inner to outer heliosphere.

[29] We examined the plasma behavior of small-scale flux ropes at 1 AU with the database of events identified with the ACE spacecraft, of which there were 70 events identified from 1998 to 2007. To understand the cumulative plasma behavior before, during, and after the event, we analyzed the events with a normalized superposed epoch analysis. The zero epoch time was defined as the inflection point of the flux rope bipolar field, found in either B_Y or B_Z GSE coordinates. We flipped the bipolar rotation such that the rotation of the bipolar field was from the negative sector to the positive sector. This helped to draw the eye to the beginning, inflection point, and end boundary of the flux rope. The duration distribution of the events is scattered from ~1 h up to 8 h, with the mean duration on the ~2 h. To understand the cumulative behavior of these events, we normalized the duration of each event to an approximate mean duration of 2 h, 1 h before the inflection point and 1 h after the inflection point. In addition to this normalization,

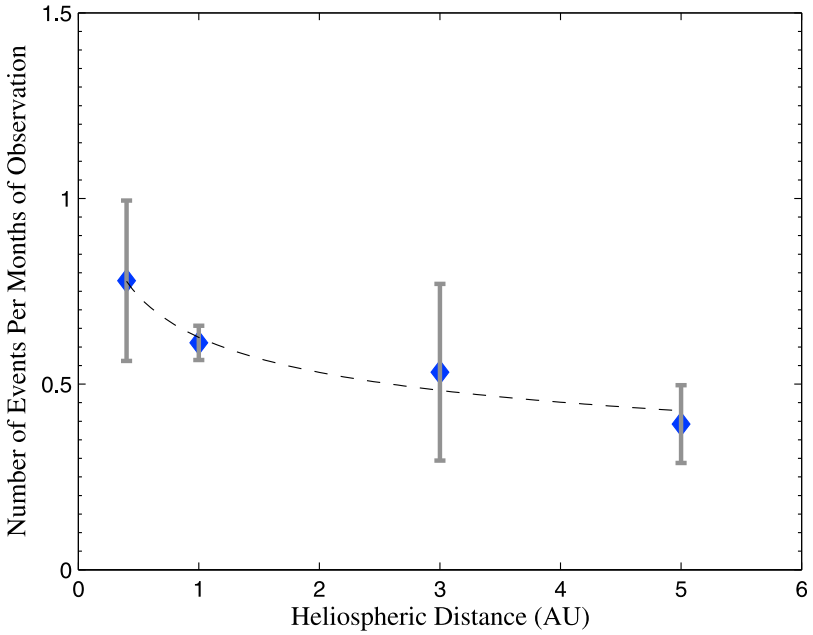

Figure 5. The number of small-scale flux ropes normalized by month of observation as a function of the radial heliospheric distance. The error bars are the square root of (the number of events) divided by the months of observation per bin. Table 1 specifies the number of months of observation per bin. The dashed line is the least squares fit, where the radial dependence is $R^{-0.24}$.

we found that in order to not have a sharp discontinuity between the boundaries of the cumulative events and the surrounding solar wind magnetic and plasma data we overlapped the normalization with part of the surrounding field and plasma data (~30 min on each side of the event). After we constructed the matrix of normalized events with the surrounding magnetic and plasma data, the upper, median, and lower quartiles were determined. The superposed epoch is presented in Figure 8. The upper level is the 75% quartile and is represented as the upper red line, the median value is the 50% quartile (the middle blue line), and the lower level is the 25% quartile (the lower red line). The first panel is the bipolar field of the flux rope, which is either in the B_Y or B_Z GSE direction. The second panel is the total magnetic field strength. The third panel is the total velocity in km s^{-1}. The total velocity is constant across the inflection point and is consistent with predominately slow solar wind (<410 km s^{-1}). The number density of protons is the fourth panel and shows a constant behavior across the inflection point. The density upper quartile shows a slight enhancement before the small-scale flux rope event, similar to the sheath region formed by swept up ambient solar wind magnetic clouds often display [*Lepping et al.*, 2006]. Beta is the ratio of plasma pressure to magnetic pressure, plotted in the fifth panel and begins to weaken at the start of the small-scale flux rope with the strongest depression at the inflection point. The total pressure is plotted in the sixth panel and is defined as the sum of the proton plasma pressure and the magnetic pressure ($P_T = n_P k T_P + B^2 / 2\mu_0$). It shows an extremely weak enhancement in the median of 0.03 nPa at the inflection point. The temperature of protons (K) is the last plot and shows a constant profile across the inflection point.

[30] We investigated the proximity of the *Wind* database of events to the nearest sector crossing (e.g., heliospheric current sheet crossing). The B_φ GSE vector is defined as starting from the Earth to the Sun, rotating counterclockwise, such that the "away" sector was at a longitude of 135° and the "toward" sector was 315°. Sector crossings were visually identified in hourly B_φ GSE vector data as a ~180 degree rotation from one sector polarity to the other. Rotations from one polarity to the other had to remain "stable" which we defined as longer than a day (e.g., if the B_φ vector rotated from one polarity to the other and then rotated back to the original polarity within a day we did not count this as a sector crossing) [*Lepping et al.*, 1996]. This was done to remove random fluctuations and ICMEs, which can disturb the heliospheric current sheet in such a manner. Sector crossings near small-scale flux ropes that were very complex and had no sustained polarity change were discarded; there were 20 events removed for this reason, leaving 71 events in the distribution. The distribution of the small-scale flux rope start time to the nearest sector crossing is presented in Figure 9. The time to sector crossing is binned is every 0.25 days. There is a very sharp peak with 17 events observed within 0.25 days of a sector crossing. The distribution has a sharp peak and is skewed with a preference before the sector crossing (skew-

Table 1. Number of Small-Scale Flux Ropes per Location and Months of Observation

Heliospheric Distance (AU)	Number of Events	Months of Observation
<0.75	13	16.7
0.75–1.5	175	286.3
1.5–4.5	5	9.4
4.5–5.5	14	35.7

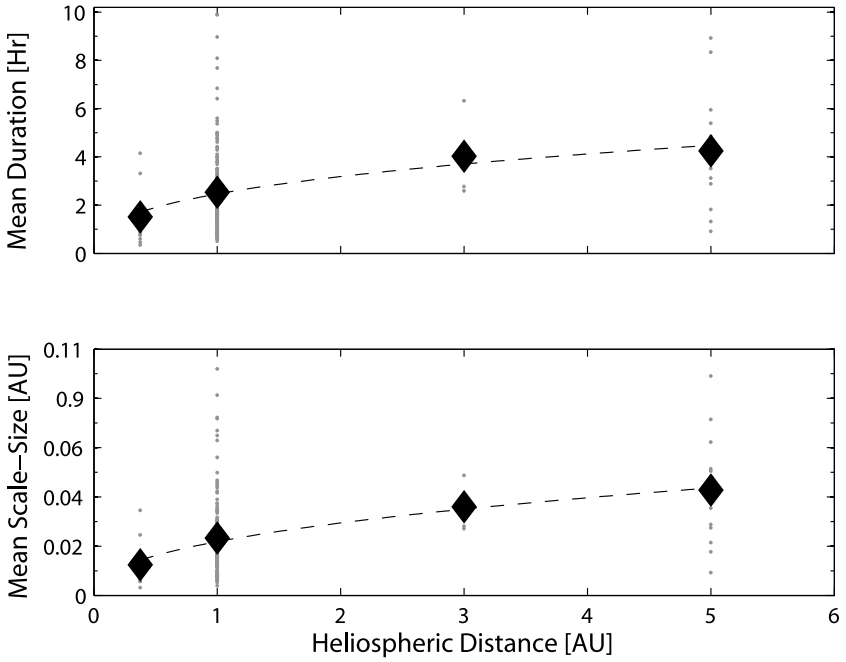

Figure 6. The top plot is the average small-scale flux rope duration per heliospheric distance binned according to Table 1, shown in black diamonds. The dashed line is the least squares fit to the data, where the radial dependence is $R^{0.37}$. The bottom plot is the average scale size of each flux rope as a function of heliospheric distance. The dashed line is the least squares fit, where the dependence is $R^{0.43}$. Each small-scale flux rope, binned per heliospheric distance, duration, and scale size, respectively, is plotted as a gray point.

ness is −0.22). The distribution has a mean of 0.016 days ± a standard deviation of 1.4 days.

4. Discussion

[31] There is a debate as to where small-scale flux ropes originate: (1) they are formed through magnetic reconnection in the solar wind such as across the heliospheric current sheet [*Moldwin et al.*, 1995, 2000; *Cartwright and Moldwin*, 2008], (2) they form in the corona similar to MCs [*Feng et al.*, 2007, 2008], or (3) there are two populations, one originating in the corona and the other in the solar wind. The evolution of small-scale flux rope properties found here can help address this debate. The first suggestion that they are created in the solar wind through reconnection [*Moldwin et al.*, 1995, 2000] was made because (1) the scale sizes of small-scale flux ropes are much smaller than MCs, (2) they lack a depressed proton temperature like MCs, and (3) they lack an expansion signature at 1 and 5.3 AU.

[32] The second hypothesis was put forth by *Feng et al.* [2007, 2008], whose studies suggest that these objects are small-scale versions of MCs with a solar origin. The reasoning was from the results of these studies at 1 AU [*Feng et al.*, 2007, 2008] using the spacecraft Wind over solar cycle 23. These results showed that small-scale flux ropes and MCs do not have strong dependence on solar cycle, both are predominately in the slow wind, have stronger core field strength as compared to the background solar wind, and their axial longitudes and latitudes are similar [*Feng et al.*, 2008]. The studies by *Feng et al.* [2007, 2008] did not remove objects from the database that were Alfvénic. This hypothesis is further supported by observations from *Mandrini et al.* [2005], who identified a sigmoid on the Sun and correlated it to a small-scale flux rope in the solar wind. This was done through timing the eruption and subsequent observation in the solar wind and comparison of the helicity of the two objects [*Mandrini et al.*, 2005]. This event was not included in our database because it was identified as an Alfvén wave. This hypothesis also does not explain why the proton temperature is not depressed in small-scale flux ropes as it is for MCs. The results from this study will help to shed light on these origin theories.

[33] Our results indicate the occurrence rate of small-scale flux ropes per year has a weak anticorrelation dependence on solar cycle. This result is consistent over three solar cycles (21–23), where on average there is 1 small-scale flux rope per month around solar minimum and 0.4 events per month around solar maximum. In comparison with large-scale flux ropes (MCs), their occurrence rate is not as dependent on the phase of the solar cycle. However, the study of ICMEs by *Richardson and Cane* [2004] found the fraction of MCs in the ICME database at solar minimum to be ~100% and at solar maximum to be ~15% during solar cycle 23. They also found that this trend was consistent in solar cycles 21 and 22. It is unclear why MCs are not as prevalent at solar maximum given the rate of ICMEs greatly increases. There have been suggestions on why MCs are less observed compared to ICMEs during solar maximum; these ideas might be related to why small-scale flux ropes are observed less during solar maximum.

[34] There are two views of why flux ropes are preferentially observed during solar minimum over ICMEs. As

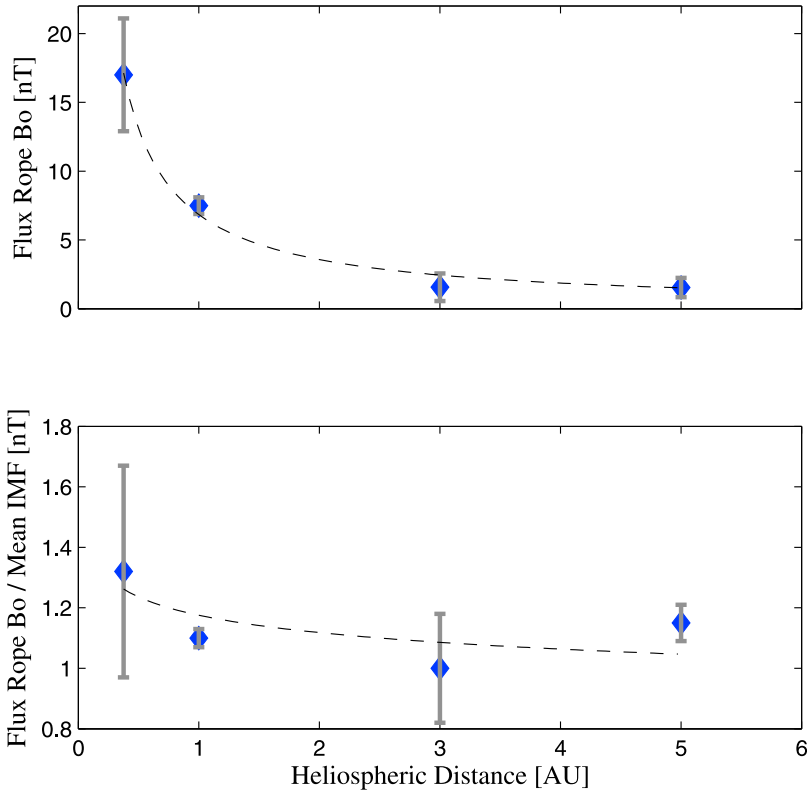

Figure 7. The top plot is the axial field strength of small-scale flux ropes versus heliospheric distance. The dashed line is the least squares fit to the data, where the radial dependence is $R^{-0.94}$. The lower plot is the axial field strength divided by the average IMF field strength of the surrounding 6 h, with the binning shown in Table 1. The dashed line is the least squares fit to the data, where the radial dependence is $R^{-0.07}$. The error bars are plus or minus the reduced error, which is the standard deviation of the average flux rope strength divided by the square root of the number of events.

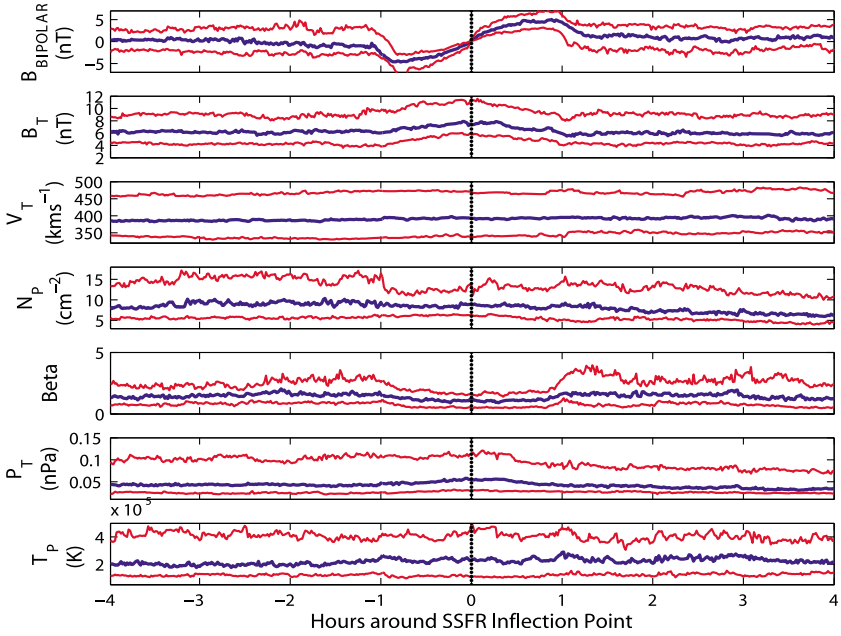

Figure 8. Superposed epoch analysis of the plasma properties of small-scale flux ropes at 1 AU.

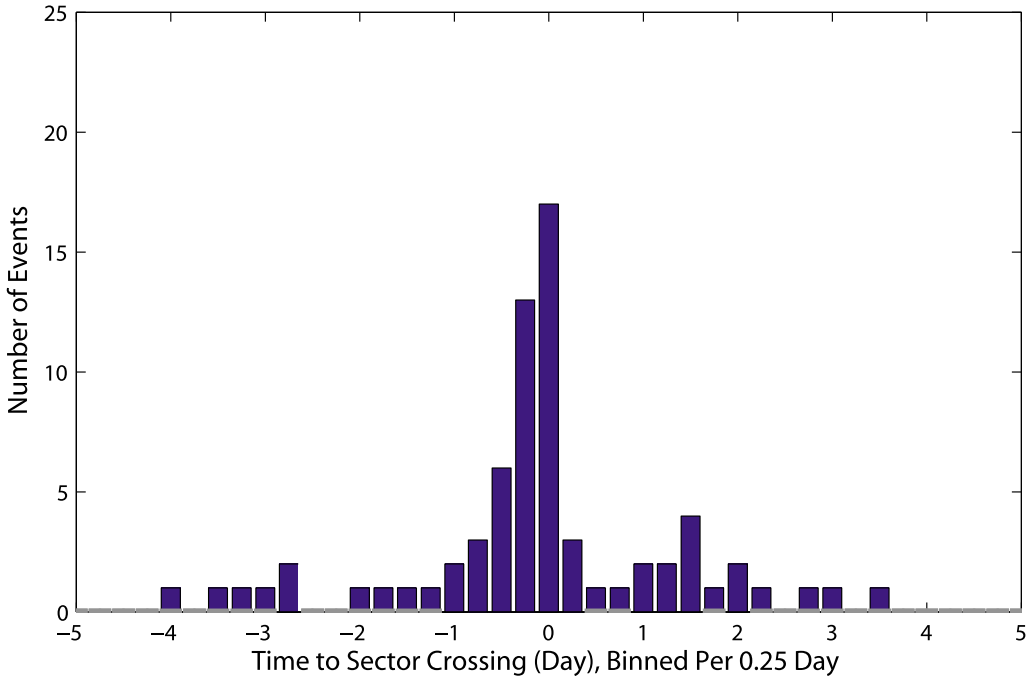

Figure 9. The distribution of events as a function of the time difference between a sector boundary crossing and a small-scale flux rope. The time to sector crossing is binned every 0.25 days, where the negative values indicate the flux rope preceded the sector crossing.

solar activity increases, the latitudinal extent of a CME core axis also increases. This term is called the apparent latitude [*Yashiro et al.*, 2004]. This could mean the magnetic clouds will only make a glancing encounter with Earth. The study by *Henke et al.* [2001] showed with Ulysses data that the percentage with high latitudes ICMEs to low latitude ICMEs increased over solar maximum. It is not clear if this is a true latitudinal change or if this is just consistent with enhanced ICME activity during solar maximum. The second view is that during solar minimum the simple flux rope configuration is more common than during solar maximum where magnetic complexity increases. *Mulligan et al.* [1998] showed higher inclination magnetic clouds are more likely to occur at solar maximum than solar minimum. There are reports of multiple flux ropes rotations within ICMEs during solar maximum [*Wu and Lepping*, 2007]. The results of this study are consistent with the view that as solar magnetic field complexity increases the occurrence of simple flux rope structure decreases. If small-scale flux ropes are being created at the Sun, then these simple force-free structures are observed more easily during solar minimum consistent with the decrease in magnetic complexity.

[35] The average number of events in the inner heliosphere is slightly greater than the outer heliosphere as seen from Figure 5. The distribution as a function of distance declines as $R^{-0.24}$. This distribution indicates the majority of events lies between 0.3 and 1 AU and then begins to declines between 1 and 5 AU. This implies the source of these small-scale flux ropes is in the inner heliosphere. This trend is more compelling when combined with the result from Figure 6 showing the increase in duration (and scale size) from the inner to outer heliosphere. The increase in duration from 0.3 to 1 AU is rapid and after 1 AU begins to flatten out. These observations suggest that small-scale flux ropes are rapidly expanding from their source in the inner heliosphere and their expansion rate slows between 1 and 5 AU.

[36] These results indicate the characteristics of small-scale flux ropes evolve as a function of heliospheric distance. As discussed in the previous paragraph, Figure 6 shows the average duration and scale size of small-scale flux ropes as a function of radial distance. The plot indicates a large, rapid expansion within 1 AU and then a much more gradual change with radial distance. The average rate of scale-size expansion varies with heliospheric distance as a function of $R^{0.43}$. This rate of expansion is weaker than the radial dependence of ICMEs, which continue to expand well past 1 AU and whose rate of expansion varies from $R^{0.5}$ to $R^{0.9}$ [*Forsyth et al.*, 2006]. The average axial core field strength of small-scale flux ropes drops off as $R^{-0.94}$ with heliospheric distance, as shown in Figure 7. This is slower than what is observed for the mean magnetic field of ICMEs, which drops as $R^{-1.3}$ to $R^{-1.5}$, as discussed in *Forsyth et al.* [2006]. Although these two parameters are not exactly the same, it is useful for comparison purposes to understand that both small-scale flux ropes and ICMEs magnetic field strength decline with radial distance. The ratio of the core field strength to the background IMF field is constant (within error bars) from the inner to outer heliosphere. The ratio is slightly greater than 1, implying small-scale flux ropes are slightly stronger than the background IMF. This suggests that these events survive out to 5.5 AU after being formed in the inner heliosphere or that they are being formed at various heliospheric distances.

[37] The superposed epoch analysis shows that small-scale flux ropes have finished their evolution at 1 AU because they are force-free, cylindrically symmetric magnetic field structures with a constant velocity profile. This is consistent with previous observations of the structure of flux

ropes at 1 AU [*Moldwin et al.*, 2000; *Feng et al.*, 2007 2008; *Cartwright and Moldwin*, 2008]. The proton temperature is constant across the duration of the event, where for magnetic clouds there is a temperature depression at 1 AU. The median of the proton density is constant across the duration of the event, giving further evidence to support the force-free nature of these events at 1 AU. The upper quartile of the proton density does show an enhancement before the event starts. This shows that there are some events that move slightly faster than the background plasma and sweep up some of the plasma in front of it creating a sheath region. This is commonly observed at the beginning of magnetic clouds. The overall behavior is best represented by the median density that remains constant across the event. The plasma beta decreases over the duration of the flux rope due to the enhancement in the total field. The total pressure shows an enhancement at the middle of the event. Since the density and temperature remain constant, the enhancement comes from the axial core field of the flux rope, which peaks at the center of the event. This total pressure peak at the center also gives further evidence of the force-free nature of these events.

[38] We investigated the solar wind context of small-scale flux ropes. We presented the time to the nearest sector crossing from the center of the small-scale flux rope in Figure 9. The results indicate that small-scale flux ropes are most often located near sector crossing (~6 h or less) and are more likely to be before the sector crossing. There are a few events found inside an ICME sheath region and the ICME itself, where the ICMEs identification is from the databases of *Jian et al.* [2008] and *Cane and Richardson* [2003]. Although we removed events that displayed compressive Alfvén wave characteristics with a correlation of 0.7, there were still approximately 10% of events that were in regions of solar wind with high shear Alfvén activity. It is possible these events are compressive Alfvén waves rather than flux ropes and could bias our results; we are working on a future study investigating these waves.

5. Conclusions

[39] This is the first investigation that observed small-scale flux ropes at a range of heliospheric radial distances, from 0.3 to 5.5 AU. We found that small-scale flux ropes are most likely to occur during solar minimum rather that solar maximum. This trend is consistent over solar cycles 21 to 23. This implies their creation mechanism is dependent on solar cycle. Their properties (occurrence, duration, and axial field strength) evolve from the inner to outer heliosphere. When combining their properties with the occurrence as a function of radial heliospheric distance, the results have shown that small-scale flux ropes are created within 1 AU. The duration of events as a function of heliospheric distance implies that there is a rapid expansion within 1 AU and they remain relatively stable to 5 AU, consistent with the events formed within 1 AU. They are most likely observed near the sector crossing.

[40] The hypothesis that small-scale flux ropes form in the corona similar to MCs [*Feng et al.*, 2007, 2008] is supported by the dependence on solar cycle and the expansion of the scale size from the inner to outer heliosphere (similar to MCs). However, if small-scale flux ropes were ejected off the Sun like magnetic clouds, then they should also have similar plasma signatures. Why do they lose their plasma signature by the time they reach 1 AU? Our results also indicate small-scale flux ropes are observed near the sector boundary crossings. This solar origin hypothesis would allow for events to be ejected from any latitude and does not explain the preference of the events to be found near the sector boundary. CMEs are regularly observed by the Large Angle Spectroscopic Coronagraph (LASCO) experiment on the SOHO satellite [*Brueckner et al.*, 1995]. If small-scale flux ropes are small magnetic clouds, it is possible to image the very largest of them being ejected off the Sun using the C1 coronagraph, but the C1 coronagraph failed early in the SOHO mission. We can extrapolate the size of small-scale flux ropes from the inner heliosphere to the Sun using the information from Figure 6. If we assume to the solar wind was on average 400 km s^{-1}, consistent with observations for small-scale flux ropes [*Cartwright and Moldwin*, 2008], and do a simple linear extrapolation of the expansion rate back to the Sun, then the scale size in the corona is between ~1 and 400 Mm. This is near the edge of the resolution range of LASCO C2 (17 Mm) and C3 (87 Mm) [*Brueckner et al.*, 1995]. However, the properties of small-scale flux ropes included in this study have different plasma and evolutionary properties from MCs and hence are consistent with a different formation mechanism suggestive that they are not just the small-sized tail of MCs.

[41] The hypothesis that they are created due to magnetic reconnection across the heliospheric current sheet [*Moldwin et al.*, 1995, 2000] is supported by our observations of being small in scale size, lacking depressed proton temperature, and that they are found near the sector crossing. The vertical extent of the heliospheric current sheet is ~10^4 km [e.g., *Winterhalter et al.*, 1994] and the average scale size of small-scale flux ropes is ~10 times this length scale. This is similar to the dimension of the magnetotail current sheet and the scale size of the tail flux ropes [e.g., *Linton and Moldwin*, 2009]. However, our results also indicate the source region is in the inner heliosphere. This does not rule out the possibility of a solar wind reconnection-type process creating these structures [*Gosling*, 2005], but it does suggest that most, if not all, are formed in the inner heliosphere.

[42] We believe our current results are most consistent with formation by (1) magnetic reconnection across the current sheet in the inner heliosphere and possibly (2) a formation mechanism; that small-scale flux ropes are remnants of the streamer belt blobs formed from disconnection [*Wang et al.*, 1998]. The streamer belt blobs are observed in the slow wind and have a bipolar structure [*Wang et al.*, 1998]. This would account for the lack of flux ropes during solar maximum when the helmet streamers are less confined to the solar equator. This hypothesis could also explain the expansion of the small-scale flux rope dimension from the inner to outer heliosphere. If they are created near the Sun and are overpressured flux ropes, then they could expand into the solar wind consistent with the observations. However, no one-to-one observation of a blob and a small-scale flux rope in the solar wind has yet been found.

Appendix A

[43] Table A1.

Table A1. Small-Scale Solar Wind Flux Rope Database

Spacecraft	Start Time (UT)	End Time (UT)
Helios 1	29 Dec 1974 1333	29 Dec 1974 1450
Helios 1	4 Mar 1975 0219	4 Mar 1975 0247
Helios 1	19 Aug 1975 2019	19 Aug 1975 2055
Helios 2	4 Mar 1976 0520	4 Mar 1976 0631
Helios 2	11 Apr 1976 1919	11 Apr 1976 2122
Helios 2	22 Nov 1976 1812	22 Nov 1976 2000
Helios 1	5 Dec 1976 0725	5 Dec 1976 0833
Helios 1	3 Jan 1977 0906	3 Jan 1977 0956
Helios 1	11 Jan 1977 0509	11 Jan 1977 0539
Helios 1	15 Jan 1977 1517	15 Jan 1977 1555
Helios 1	27 Jan1977 0140	27 Jan 1977 0325
Helios 2	19 Feb 1977 2303	20 Feb 1977 0403
Helios 2	16 Mar 1977 1430	16 Mar 1977 1523
Helios 1	22 Mar 1977 1001	22 Mar 1977 1022
Helios 1	14 Apr 1977 1725	14 Apr 1977 2134
Helios 2	29 Oct 1977 1823	29 Oct1977 2002
Helios 1	6 Dec 1978 1302	06 Dec 1978 1349
Helios 1	19 Jan 1979 1832	19 Jan 1979 2019
Helios 2	25 Nov 1979 0912	25 Nov 1979 0957
Helios 2	30 Dec 1979 1732	30 Dec 1979 1956
Helios 1	2 Jan 1980 1313	2 Jan 1980 1632
Helios 1	16 Jan 1980 1220	16 Jan 1980 1422
Helios 1	14 May 1980 0815	14 May 1980 0958
IMP 8	29 May 1975 1510	29 May 1975 1552
IMP 8	7 Jun 1975 0752	7 Jun 1975 0919
IMP 8	18 Jan 1976 0548	18 Jan 1976 0654
IMP 8	22 Jan 1976 0419	22 Jan 1976 0514
IMP 8	26 Feb 1976 1712	26 Feb 1976 1750
IMP 8	21 Oct 1976 2057	21 Oct 1976 2145
IMP 8	7 Nov 1976 0004	07 Nov 1976 0421
IMP 8	14 Apr 1977 0723	14 Apr 1977 0904
IMP 8	27 Apr 1977 1051	27 Apr 1977 1217
IMP 8	25 Dec 1977 1852	25 Dec 1977 2104
IMP 8	2 Jan 1978 0430	2 Jan 1978 0508
IMP 8	19 Jan 1978 0107	19 Jan 1978 0449
IMP 8	16 Jun 1978 1541	16 Jun 1978 1719
IMP 8	20 Jul 1979 0426	20 Jul 1979 0531
IMP 8	20 Sep 1979 1443	20 Sep 1979 1737
IMP 8	15 Jan 1980 2230	16 Jan 1980 0037
IMP 8	24 Jan 1980 0840	24 Jan 1980 0933
IMP 8	21 Feb 1980 2102	22 Feb 1980 0128
IMP 8	19 Mar 1980 0617	19 Mar 1980 0745
IMP 8	28 Mar 1980 2232	29 Mar 1980 0012
IMP 8	6 May 1980 0937	6 May 1980 1109
IMP 8	31 Oct 1981 2018	31 Oct 1981 2232
IMP 8	19 May 1982 1825	19 May 1982 1918
IMP 8	6 Oct 1982 1236	06 Oct 1982 1642
IMP 8	31 Oct 1982 2234	1 Nov 1982 0113
IMP 8	24 Nov 1982 2241	25 Nov 1982 0053
IMP 8	3 Jan 1983 1832	3 Jan 1983 1859
IMP 8	11 May 1983 1739	11 May 1983 1831
IMP 8	24 Jul 1983 0945	24 Jul 1983 1214
IMP 8	6 Oct 1983 0931	6 Oct 1983 1206
IMP 8	14 Jan 1984 2239	14 Jan 1984 2247
IMP 8	15 Jan 1985 2140	15 Jan 1985 2322
IMP 8	21 Mar 1985 1629	21 Mar 1985 1938
IMP 8	22 Mar 1985 2154	23 Mar 1985 0014
IMP 8	30 Mar 1985 1346	30 Mar 1985 1437
IMP 8	31 Mar 1985 1019	31 Mar 1985 1223
IMP 8	25 Apr 1985 0658	25 Apr 1985 0840
IMP 8	6 May 1985 0343	6 May 1985 0419
IMP 8	11 May 1985 0746	11 May 1985 0851
IMP 8	1 Jun 1985 0640	1 Jun 1985 0802
IMP 8	2 Jun 1985 2051	2 Jun 1985 2144
IMP 8	4 Jun 1985 2047	5 Jun 1985 0053
IMP 8	1 Nov 1985 1807	1 Nov 1985 2001
IMP 8[a]	13 Apr 1986 0724	13 Apr 1986 1524
IMP 8	22 Apr 1986 0904	22 Apr 1986 1043
IMP 8	24 Jul 1986 2107	24 Jul 1986 2310
IMP 8	5 Oct 1986 0827	5 Oct 1986 1035
IMP 8	18 Oct 1986 0741	18 Oct 1986 0824
IMP 8	10 Dec 1986 1855	10 Dec 1986 1951
IMP 8	12 Jan 1987 0929	12 Jan 1987 1102
IMP 8	6 Feb 1987 1020	6 Feb 1987 1113
IMP 8	30 Mar 1987 2014	31 Mar 1987 0219
IMP 8	2 Nov 1987 1800	2 Nov 1987 1900
IMP 8	11 Feb 1988 2018	11 Feb 1988 2145
IMP 8	6 Mar 1988 1755	6 Mar 1988 2026
IMP 8	26 Apr 1988 2231	27 Apr 1988 0116
IMP 8	3 Mar 1989 0529	03 Mar 1989 0711
IMP 8	10 Jul 1989 0346	10 Jul 1989 0640
IMP 8	6 Feb 1990 1820	06 Feb 1990 2213
IMP 8	25 Jan 1991 1616	25 Jan 1991 1714
IMP 8	24 Apr 1992 2331	25 Apr 1992 0022
IMP 8	15 Aug 1992 0206	15 Aug 1992 0649
IMP 8	9 Sep 1992 1050	09 Sep 1992 1434
IMP 8	21 Dec 1992 2043	21 Dec 1992 2206
IMP 8	11 Feb 1993 0030	11 Feb 1993 0137
IMP 8	15 Aug 1994 2116	15 Aug 1994 2343
Wind	14 Jan 1995 0547	14 Jan 1995 0853
Wind	21 Feb 1995 1921	21 Feb 1995 2116
Wind	24 Mar 1995 0250	24 Mar 1995 0648
Wind	24 Mar 1995 1123	24 Mar 1995 1623
Wind	2 May 1995 0447	2 May 1995 0540
Wind	16 May 1995 0111	16 May 1995 0917
Wind	7 Jun 1995 0938	7 Jun 1995 1836
Wind	19 Jun 1995 0110	19 Jun 1995 0206
Wind	4 Jul 1995 0259	4 Jul 1995 0500
Wind	11 Aug 1995 0418	11 Aug 1995 0557
Wind	15 Aug 1995 1418	15 Aug 1995 1719
Wind	17 Aug 1995 2027	18 Aug 1995 0157
Wind	19 Sep 1995 1849	19 Sep 1995 1946
Wind	20 Sep 1995 1259	20 Sep 1995 1414
Wind	21 Sep 1995 0252	21 Sep 1995 0454
Wind	27 Sep 1995 1349	27 Sep 1995 2130
Wind	24 Oct 1995 1309	24 Oct 1995 1409
Wind	27 Oct 1995 1035	27 Oct 1995 1138
Wind	3 Dec 1995 0402	3 Dec 1995 0541
Wind	13 Mar 1996 0924	13 Mar 1996 1044
Wind	16 Mar 1996 2227	17 Mar 1996 0228
Wind	19 Mar 1996 0902	19 Mar 1996 0956
Wind	11 Apr 1996 1314	11 Apr 1996 1447
Wind	14 Apr 1996 1052	14 Apr 1996 1228
Wind	14 May 1996 2154	14 May 1996 2313
Wind	11 Aug 1996 2059	12 Aug 1996 0136
Wind	23 Aug 1996 0243	23 Aug 1996 0550
Wind	29 Aug 1996 0121	29 Aug 1996 0211
Wind	11 Nov 1996 1636	11 Nov 1996 1952
Wind	28 Jan 1997 0217	28 Jan 1997 0547
Wind	23 Mar 1997 1212	23 Mar 1997 1339
Wind	9 May 1997 0323	9 May 1997 0846
Wind	24 Jul 1997 0727	24 Jul 1997 0907
Wind	2 Sep 1997 0231	2 Sep 1997 0654
Wind	6 Jan 1998 1959	6 Jan 1998 2215
Wind	16 Jan 1998 1128	16 Jan 1998 1311
Wind/ACE[b]	1 Feb 1998 0050	1 Feb 1998 0626
Wind/ACE	23 Feb 1998 1534	23 Feb 1998 1748
Wind/ACE	27 Feb 1998 0534	27 Feb 1998 0846
Wind/ACE	20 Mar 1998 1442	20 Mar 1998 1712
Wind/ACE	10 Jun 1998 2236	10 Jun 1998 2347
Wind/ACE	10 Jul 1998 2246	11 Jul 1998 0858
Wind/ACE	6 Nov 1998 2158	6 Nov 1998 2324
Wind/ACE	3 Feb 1999 0924	3 Feb 1999 1201
ACE	3 Feb 1999 1206	3 Feb 1999 1351
ACE	4 Feb 1999 1010	4 Feb 1999 1318
Wind/ACE	11 Feb 1999 0011	11 Feb 1999 0333
ACE	25 Mar 1999 1608	25 Mar 1999 2259
ACE	23 Apr 1999 0537	23 Apr 1999 0829
Wind/ACE	24 May 1999 0900	24 May 1999 1045
Wind/ACE	27 Jun 1999 1117	27 Jun 1999 1156
Wind/ACE	6 Aug 1999 1029	6 Aug 1999 1225
Wind/ACE	11 Aug 1999 0010	11 Aug 1999 0416
ACE	17 Nov 1999 1608	17 Nov 1999 1659
Wind/ACE	28 Dec 1999 0626	28 Dec 1999 0807

Table A1. (continued)

Spacecraft	Start Time (UT)	End Time (UT)
Wind/ACE	27 Apr 2000 1850	27 Apr 2000 2347
Wind/ACE	19 Jul 2000 2117	20 Jul 2000 0043
Wind/ACE	12 Aug 2000 0220	12 Aug 2000 0526
Wind/ACE	1 Oct 2000 1924	1 Oct 2000 2242
Wind/ACE	29 Dec 2000 0115	29 Dec 2000 0326
ACE	18 Feb 2001 2136	18 Feb 2001 2328
Wind/ACE	31 Mar 2001 0606	31 Mar 2001 1231
Wind	18 May 2001 0952	18 May 2001 1323
Wind/ACE	9 Jun 2001 0314	9 Jun 2001 0500
Wind/ACE	10 May 2002 1709	10 May 2002 2006
Wind/ACE	7 Jun 2002 1918	7 Jun 2002 2318
Wind/ACE	19 Jun 2002 0249	19 Jun 2002 0340
Wind/ACE	7 Jul 2003 0322	7 Jul 2003 0442
Wind/ACE	9 Jun 2004 0649	9 Jun 2004 0915
Wind/ACE	9 Jul 2004 0535	9 Jul 2004 0922
Wind/ACE	9 Aug 2004 0201	9 Aug 2004 0648
Wind/ACE	14 Sep 2004 1634	14 Sep 2004 2127
Wind/ACE	8 Oct 2004 0705	8 Oct 2004 0840
Wind/ACE	7 Jan 2005 1155	7 Jan 2005 1357
Wind/ACE	7 Jan 2005 2046	8 Jan 2005 0707
Wind	10 Jan 2005 2255	10 Jan 2005 2341
Wind	14 Jan 2005 1722	14 Jan 2005 1959
Wind/ACE	5 Mar 2005 0727	5 Mar 2005 0929
Wind/ACE	31 May 2005 1925	31 May 2005 2218
Wind/ACE	24 Aug 2005 0823	24 Aug 2005 1027
Wind/ACE	31 Aug 2005 1534	31 Aug 2005 1701
Wind/ACE	30 Sep 2005 1041	30 Sep 2005 1231
Wind/ACE	14 Jan 2006 1739	14 Jan 2006 1931
Wind/ACE	22 Jan 2006 1249	22 Jan 2006 1502
Wind/ACE	19 Feb 2006 0351	19 Feb 2006 0719
Wind/ACE	8 Apr 2006 0733	8 Apr 2006 0919
Wind/ACE	30 May 2006 1339	30 May 2006 1605
Wind/ACE	24 Jun 2006 2309	25 Jun 2006 0142
Wind	26 Jul 2006 1727	26 Jul 2006 1854
Wind/ACE	12 Sep 2006 0128	12 Sep 2006 0515
Wind/ACE	28 Jan 2007 0017	28 Jan 2007 0316
Wind/ACE	19 Feb 2007 1029	19 Feb 2007 1212
Wind/ACE	1 Mar 2007 1611	1 Mar 2007 1654
ACE	12 Mar 2007 1229	12 Mar 2007 1314
Wind/ACE	18 Apr 2007 2118	18 Apr 2007 2234
Wind/ACE	15 Jul 2007 0117	15 Jul 2007 0157
Wind/ACE	30 Sep 2007 2054	30 Sep 2007 2205
Wind/ACE	30 Nov 2007 1159	30 Nov 2007 1414
Ulysses	3 Nov 1990 0731	3 Nov 1990 0812
Ulysses	28 Jan 1991 1003	28 Jan 1991 1623
Ulysses	24 Apr 1991 0550	24 Apr 1991 1015
Ulysses	25 Apr 1991 1416	25 Apr 1991 1642
Ulysses	8 May 1991 1335	8 May 1991 1621
Ulysses	27 Jun 1991 2237	28 Jun 1991 0113
Ulysses	5 Nov 1991 0540	5 Nov 1991 1137
Ulysses	27 Apr 1992 0032	27 Apr 1992 0339
Ulysses	23 May 1992 0707	23 May 1992 1158
Ulysses	21 Jun 1992 2242	22 Jun 1992 0447
Ulysses	15 Jul 1992 0821	15 Jul 1992 1015
Ulysses	1 Aug 1992 2038	2 Aug 1992 0009
Ulysses	25 Jan 1998 1613	26 Jan 1998 0034
Ulysses	20 Jan 2004 0940	20 Jan 2004 1035
Ulysses	16 Jun 2004 1329	16 Jun 2004 1622
Ulysses	13 Jul 2004 0735	13 Jul 2004 1630
Ulysses	4 Aug 2004 0306	4 Aug 2004 0830
Ulysses	28 Nov 2004 0605	28 Nov 2004 0755
Ulysses	10 Dec 2004 0745	10 Dec 2004 1139
Ulysses	27 Jan 2005 1842	27 Jan 2005 2002

[a]This flux rope had a small data gap (5% of total duration) that was linearly interpolated across.

[b]When the flux rope was found by Wind and ACE, the time at Wind was used.

[44] **Acknowledgments.** We would like to thank the magnetic field and plasma data set teams for their careful work: PIs Ness, Neubauer, and Rosenbauer for Helios 1 and Helios 2 data sets; PIs Lepping and Lazarus for the IMP 8 data set; the Wind spacecraft MFI (PI: Lepping) and SWE (PIs: Ogilvie and Lazarus) teams; the ACE MAG (PI: Ness) and SWEPAM (Los Alamos) teams; and the Ulysses magnetic field team (PI: Balogh) and the plasma team SWOOPS (PI: Bame). We also thank the referees for their helpful comments that greatly improved the paper. We would like to thank the National Space Science Data Center and the Space Physics Data Facility for making all the data sets publicly available. We thank J. Weygand for the use of the solar wind data set he has carefully compiled. This work was supported by NASA SR&T (NAG5-12823) and a NASA Goddard Space Flight Center GSRP Fellowship.

[45] Zuyin Pu thanks Ian Richardson and another reviewer for their assistance in evaluating this paper.

References

Balogh, A., T. J. Beek, R. J. Forsyth, P. C. Hedgecock, R. J. Marquedant, E. J. Smith, D. J. Southwood, and B. T. Tsurutani (1992), The magnetic field investigation on the ULYSSES mission—Instrumentation and preliminary scientific results, *Astron. Astrophys. Suppl. Ser.*, *92*, 221–236.

Bame, S. J., D. J. McComas, B. L. Barraclough, J. L. Phillips, K. J. Sofaly, J. C. Chavez, B. E. Goldstein, and R. K. Sakurai (1992), The ULYSSES solar wind plasma experiment, *Astron. Astrophys. Suppl. Ser.*, *92*, 237–265.

Bothmer, V., and D. M. Rust (1997), The field configuration of magnetic clouds and the solar cycle, in *Coronal Mass Ejections*, *Geophys. Monogr. Ser.*, vol. 99, edited by N. Crooker et al., pp. 139–146, AGU, Washington, D. C.

Bothmer, V., and R. Schwenn (1998), The structure and origin of magnetic clouds in the solar wind, *Ann. Geophys.*, *16*, 1–24.

Brueckner, G. E., R. A. Howard, M. J. Kooman, C. M. Korendyke, D. J. Michels, J. D. Moses, D. G. Socker, K. P. Dere, P. L. Lamy, A. Llebaria, et al. (1995), The large angle spectroscopic coronagraph (LASCO), *Sol. Phys.*, *162*, 357–402.

Bruno, R., B. Bavassano, and U. Villante (1985), Evidence for long period Alfvén waves in the inner solar system, *J. Geophys. Res.*, *90*(A5), 4373–4377, doi:10.1029/JA090iA05p04373.

Burlaga, L., E. Sittler, F. Mariani, and R. Schwenn (1981), Magnetic loop behind an interplanetary shock-Voyager, Helios, and IMP 8 observations, *J. Geophys. Res.*, *86*, 6673–6684.

Burlaga, L. F. (1988), Magnetic clouds and force-free fields with constant alpha, *J. Geophys. Res.*, *93*(A7), 7217–7224.

Burlaga, L. F., and K. W. Behannon (1982), Magnetic clouds: Voyage observations between 2 and 4 AU, *Sol. Phys.*, *81*, 181–192, doi:10.1007/BF00151989.

Burlaga, L. F., and J. M. Turner (1976), Microscale "Alfvén waves" in the solar wind at 1 AU, *J. Geophys. Res.*, *81*(1) 73–77, doi:10.1029/JA081i001p00073.

Cane, H. V., and I. G. Richardson (2003), Interplanetary coronal mass ejections in the near-Earth solar wind during 1996–2002, *J. Geophys. Res.*, *108*(A4), 1156, doi:10.1029/2002JA009817.

Cartwright, M. L., and M. B. Moldwin (2008), Comparison of small-scale flux rope magnetic properties to large-scale magnetic clouds: Evidence for reconnection across the HCS?, *J. Geophys. Res.*, *113*, A09105, doi:10.1029/2008JA013389.

Farrugia, C. F., V. A. Osherovich, and L. F. Burlaga (1995), The magnetic flux rope versus the spheromak as models for interplanetary magnetic clouds, *J. Geophys. Res.*, *100*(A7), 12,293–12,306, doi:10.1029/95JA00272.

Feng, H. Q., D. J. Wu, and J. K. Chao (2007), Size and energy distributions of interplanetary magnetic flux ropes, *J. Geophys. Res.*, *112*, A02102, doi:10.1029/2006JA011962.

Feng, H. Q., D. J. Wu, C. C. Lin, J. K. Chao, L. C. Lee, and L. H. Lyu (2008), Interplanetary small-and intermediate-sized magnetic flux ropes during 1995–2005, *J. Geophys. Res.*, *113*, A12105, doi:10.1029/2008JA013103.

Forsyth, R. J., V. Bothmer, C. Cid, N. U. Crooker, T. S. Horbury, K. Kecskemety, B. Klecker, J. A. Linker, D. Odstrcil, M. J. Reiner, et al. (2006), ICMEs in the inner heliosphere: Origin, evolution and propagation effects. Report of Working Group G, *Space Sci. Rev.*, *123*(1–3), 383, doi:10.1007/s11214-006-9022-0.

Goldstein, H. (1983), On the field configuration in magnetic clouds, in *Solar Wind Five*, edited by M. Neugebauer, *NASA Conf. Publ.*, *CP-2280*, 731–733.

Gosling, J. T. (2005), Magnetic reconnection in the solar wind: A brief overview, in *Proceedings of the Solar Wind 11/SOHO 16* "*Connecting*

Sun and Heliosphere" *Conference (ESA SP-592)*, edited by B. Fleck et al., p. 249, 12–17 June 2005, Whistler, Canada.

Henke, T., J. Woch, R. Schwenn, U. Mall, G. Gloeckler, R. von Steiger, R. J. Forsyth, and A. Balogh (2001), Ionization state and magnetic topology of coronal mass ejections, *J. Geophys. Res.*, *106*(A6), doi:10.1029/2000JA900176.

Jian, L., C. T. Russell, J. G. Luhmann, R. M. Skoug, and J. T. Steinberg (2008), Stream interactions and interplanetary coronal mass ejections at 5.3 AU near the solar ecliptic plane, *Solar Phys.*, *250*(2), 375–402, doi:10.1007/s11207-008-904-x.

Klein, L. W., and L. F. Burlaga (1982), Interplanetary magnetic clouds at 1 AU, *J. Geophys. Res.*, *87*(A2), 613–624, doi:10.1029/JA087iA02p00613.

Lepping, R. P., and C.-C. Wu (2007), On the variation of interplanetary magnetic cloud type through solar cycle 23: Wind events, *J. Geophys. Res.*, *112*, A10103, doi:10.1029/2006JA012140.

Lepping, R. P., L. F. Burlaga, and J. A. Jones (1990), Magnetic field structure of interplanetary magnetic clouds at 1 AU, *J. Geophys. Res.*, *95*(A8), 11,957–11,965, doi:10.1029/JA095iA08p11957.

Lepping, R. P., et al. (1995), The WIND magnetic field investigation, *Space Sci. Rev.*, *71*(1–4), 207–209, doi:10.1007/BF00751330.

Lepping, R. P., A. Szabo, M. Peredo, and J. T. Hoeksema (1996), Large-scale properties and solar connection of the heliospheric current and plasma sheets: WIND observations, *Geophys. Res. Lett.*, *23*(10), 1199–1202, doi:10.1029/96GL00658.

Lepping, R. P., D. B. Berdichevsky, C.-C. Wu, A. Szabo, T. Narock, F. Mariani, A. J. Lazarus, and A. J. Quivers (2006), A summary of WIND magnetic clouds for years 1995–2003: Model-fitted parameters, associated errors and classifications, *Ann. Geophys.*, *24*(1), 215–245, doi:10.5194/angeo-24-215-2006.

Linton, M. G., and M. B. Moldwin (2009), A comparison of the formation and evolution of magnetic flux ropes in solar coronal mass ejections and magnetotail plasmoids, *J. Geophys. Res.*, *114*, A00B09, doi:10.1029/2008JA013660.

Lundquist, S. (1950), Magnetohydrostatic fields, *Ark. Phys.*, *2*, 361–365.

Lynch, B. J., J. R. Gruesbeck, and T. H. Zurbuchen (2005), Solar cycle-dependent helicity transport by magnetic clouds, *J. Geophys. Res.*, *110*, A08107, doi:10.1029/2005JA011137.

Mandrini, C. H., et al. (2005), The smallest source region of an interplanetary magnetic cloud: A mini-sigmoid, *Adv. Space Sci.*, *36*, 1579–1586.

McComas, D. J., S. J. Bame, P. Barker, W. C. Feldman, J. L. Phillips, P. Riley, and J. W. Griffee (1998), Solar wind electron proton alpha monitor (SWEPAM) for the Advanced Composition Explorer, *Space Sci. Rev.*, *86*, 563, doi:10.1023/A:1005040232597.

Moldwin, M. B., and W. J. Hughes (1992), On the formation and evolution of plasmoids—A survey of ISEE 3 Geotail data, *J. Geophys. Res.*, *97*(A12), 19,259–19,282.

Moldwin, M. B., J. L. Phillips, J. T. Gosling, E. E. Scime, D. J. McComas, S. J. Bame, A. Balogh, and R. J. Forsyth (1995), Ulysses observations of a noncoronal mass ejection flux rope: Evidence of interplanetary magnetic reconnection, *J. Geophys. Res.*, *100*(10), 19,903–19,910, doi:10.1029/95JA01123.

Moldwin, M. B., S. Ford, R. Lepping, J. Slavin, and A. Szabo (2000), Small-scale magnetic flux ropes in the solar wind, *Geophys. Res. Lett.*, *27*(1), 57–60, doi:10.1029/1999GL010724.

Mulligan, T., C. T. Russell, and J. Luhmann (1998), Solar cycle evolution of the structure of magnetic clouds in the inner heliosphere, *Geophys. Res. Lett.*, *25*(15), 2959–2962, doi:10.1029/98GL01302.

Mulligan, T. L. (2002), The structure of interplanetary coronal mass ejections and their solar origins, Ph.D. dissertation, 370 pp., Univ. of Calif., Los Angeles.

Ogilvie, K. W., D. J. Chornay, R. J. Fritzenreiter, F. Hunsaker, J. Keller, J. Lobell, G. Miller, J. D. Scudder, E. C. Sittler Jr., R. B. Torbert, et al. (1995), SWE, a comprehensive plasma instrument for the WIND, *Space Sci. Rev.*, *71*, 55, doi: 10.1007/BF00751326.

Osherovich, V., J. Fainberg, and R. Stone (1999), Multi-tube model for interplanetary magnetic clouds, *Geophys. Res. Lett.*, *26*(3), 401–404, doi:10.1029/1998GL900306.

Richardson, I. G., and H. V. Cane (2004), The fraction of interplanetary coronal mass ejections that are magnetic clouds: Evidence for a solar cycle variation, *Geophys. Res. Lett.*, *31*, L18804, doi:10.1029/2004GL020958.

Rosenbauer, H., R. Schwenn, E. Marsh, B. Meyer, H. Miggenrieder, M. D. Montgomery, K. H. Mulhauser, W. Phillip, W. Voges, and S. M. Zink (1977), A survey on initial results of the Helios plasma experiment, *J. Geophys. Res.*, *42*, 561–580.

Scearce, C., S. Cantarano, N. Ness, F. Mariani, R. Terenzi, and L. Burlaga (1975), Rome-GSFC magnetic field experiment for Helios A and B (E3), *Raumfahrtforschung*, *19*, 237–240.

Smith, C. W., J. L'Heureux, N. F. Ness, M. H. Acuña, L. F. Burlaga, and J. Scheifele (1998), The ACE magnetic fields experiment, *Space Sci. Rev.*, *86*, 613, doi:10.1023/A:1005092216668.

Smith, E. J., A. Balogh, M. Neugebauer, and D. McComas (1995), Ulysses observations of Alfvén waves in the southern and northern solar hemispheres, *Geophys. Res. Lett.*, *22*(23), 3381–3384, doi:10.1029/95GL03268.

Sonnerup, B. U. O., and L. J. Cahill (1967), Magnetopause structure and attitude from Explorer 12 observations, *J. Geophys. Res.*, *72*(1), 171–183, doi:10.1029/JZ072i001p00171.

Vandas, M., S. Fisher, P. Pelant, and A. Geranios (1993), Spheriodal models of magnetic clouds and their comparison with spacecraft measurements, *J. Geophys. Res.*, *98*(A7), 11,467–11,475, doi:10.1029/93JA00055.

Wang, Y.-M., N. R. Sheeley Jr., J. H. Walters, G. E. Brueckner, R. A. Howard, and D. J. Michels (1998), Origin of streamer material in the outer corona, *APJ*, *498*, L165–L168.

Winterhalter, D., E. J. Smith, M. E. Burton, N. Murphy, and D. J. McComas (1994), The heliospheric plasma sheet, *J. Geophys. Res.*, *99*(A4), 6667–6680, doi:10.1029/93JA03481.

Wu, C.-C., and R. P. Lepping (2007), Comparison of the Characteristics of Magnetic Clouds and Magnetic Cloud-like Structures for the Events of 1995–2003, *Solar Phys.*, *242*, 159–165, doi:10.1007/s11207-007-0323-6.

Yashiro, S., N. Gopalswamy, G. Michalek, O. C. St. Cyr, S. P. Plunkett, N. B. Rich, and R. A. Howard (2004), A catalog of white light coronal mass ejections observed by the SOHO spacecraft, *J. Geophys. Res.*, *109*, A07105, doi:10.1029/2003JA010282.

M. L. Cartwright, Space Sciences Laboratory, University of California, 7 Gauss Way, Berkeley, CA 94720-7450, USA. (mcartwright@ssl.berkeley.edu)

M. B. Moldwin, Department of Atmospheric, Oceanic, and Space Sciences, University of Michigan, Space Research Bldg., 2455 Hayward St., Ann Arbor, MI 48109-2143, USA.